

2024

## Air Jet Assisted Combustion of Oil Diffusion Flames: Effects of Injection Location and Excess Air Factor

Moustafa Ahmed GamalEldin

*Continuous Combustion Laboratory, Mechanical Power Engineering Department, Faculty of Engineering - Mataria, Helwan University, Cairo 11718, Egypt, moustafaahmed1411@gmail.com*

Neama Youssef Ramadan

*Continuous Combustion Laboratory, Mechanical Power Engineering Department, Faculty of Engineering - Mataria, Helwan University, Cairo 11718, Egypt*

Ahmed Mohamed Abdulnaim

*Continuous Combustion Laboratory, Mechanical Power Engineering Department, Faculty of Engineering - Mataria, Helwan University, Cairo 11718, Egypt, ahmed-abdulnaim@m-eng.helwan.edu.eg*

Ahmed Abdelnasser Adam

*Continuous Combustion Laboratory, Mechanical Power Engineering Department, Faculty of Engineering - Mataria, Helwan University, Cairo 11718, Egypt*

Ahmed Abdulrazik Emara

*Continuous Combustion Laboratory, Mechanical Power Engineering Department, Faculty of Engineering - Mataria, Helwan University, Cairo 11718, Egypt*



Part of the [Heat Transfer, Combustion Commons](https://tast.researchcommons.org/journal)

*See next page for additional authors*

### How to Cite This Article

GamalEldin, Moustafa Ahmed; Ramadan, Neama Youssef; Abdulnaim, Ahmed Mohamed; Adam, Ahmed Abdelnasser; Emara, Ahmed Abdulrazik; and Moneib, Hany Ahmed (2024) "Air Jet Assisted Combustion of Oil Diffusion Flames: Effects of Injection Location and Excess Air Factor," *Trends in advanced sciences and technology*. Vol. 1: Iss. 1, Article 4.

DOI: 10.62537/2974-444X.1003

Available at: <https://tast.researchcommons.org/journal/vol1/iss1/4>

This Original Study is brought to you for free and open access by Trends in Advanced Sciences and Technology. It has been accepted for inclusion in Trends in advanced sciences and technology by an authorized editor of Trends in Advanced Sciences and Technology.

---

# Air Jet Assisted Combustion of Oil Diffusion Flames: Effects of Injection Location and Excess Air Factor

## Authors

Moustafa Ahmed GamalEldin, Neama Youssef Ramadan, Ahmed Mohamed Abdulnaim, Ahmed Abdelnasser Adam, Ahmed Abdulrazik Emara, and Hany Ahmed Moneib

## ORIGINAL STUDY

# Air-jet-assisted Combustion of Oil Diffusion Flames: Effects of Injection Location and Excess Air Factor

Moustafa Ahmed GamalEldin<sup>\*</sup>, Neama Youssef Ramadan, Ahmed Mohamed Abdalnaim, Ahmed Abdelnasser Adam, Ahmed Abdulrazik Emara, Hany Ahmed Moneib

Continuous Combustion Laboratory, Department of Mechanical Power Engineering, Faculty of Engineering – Mataria, Helwan University, Cairo, Egypt

## Abstract

Oil diffusion flames are used in diverse industrial applications. Their characteristics, stability, and exhaust emissions are very much dependent on the way and the degree of mixing. In that respect they suffered from the existence of a sooty base due to the slower rate of fuel vaporization together with the deficiency of oxidant availability at the flame core region (yellowish color), leading to high exhaust emissions of unburned hydrocarbons and CO. Nonetheless, their stabilization through a central recirculation zone (via a stabilizer disk or a vane swirler) results in the elongation of the reactants residence time, resulting in the creation of local hot spots, giving higher NO<sub>x</sub> exhaust emissions. The present paper introduces a new methodology that relied on the incorporation of multiple air injection jets onto the spray flame core base region to accelerate fuel vaporization and rapid mixture formation to improve the overall combustion efficiency and exhaust emissions. In that respect, focus is given to examining the optimum location of the air injection jets (at a fixed load, constant jet momentum, and angle). Results demonstrate significant improvements in oil diffusion flame performance through reduced flame length, temperature uniformity, soot oxidation, and lower pollutant emissions. The combustion mode shifts from a diffusion flame to a lean partially premixed flame, or a moderate or intense low-oxygen dilution combustion regime based on air injection jet parameters. The optimal location for air injection jets is found to be at the exit plane of the premix chamber (5 cm from the stabilizer disk). This injection position is associated with superior combustion efficiency, minimized carbon monoxide emissions, and a permissible level of nitrogen oxide (NO<sub>x</sub>) emissions. While applicable to gas turbine combustion and other oil diffusion flames, further studies and simulations are necessary to optimize and validate this promising technique.

**Keywords:** Air-jet-assisted combustion, Disk stabilized burner, Jet in crossflow, Jet mixing, Lean partially premixed flame, Moderate intense low oxygen dilution combustion, Oil diffusion flames

## 1. Introduction

The predominant reliance on fossil fuels for energy, despite being a major source of air pollution and global warming, has led to the development of combustion equipment conforming to strict emission standards. Notably, emission limits for carbon monoxide (CO), unburned hydrocarbons (UHC), and nitrogen oxides (NO<sub>x</sub>) vary globally, with the United States and the European Union setting specific limits (Alan et al., 2001). In

parallel, NO<sub>x</sub> should be reduced by 90% compared with a typical aircraft flying in 2000 (Dareck et al., 2011). China has recently restricted NO<sub>x</sub> emissions from coal-fired plants down to 50 mg/m<sup>3</sup> (@ 6% O<sub>2</sub>) (Li et al., 2017). The reduction of NO<sub>x</sub> emissions, achieved through lean mixtures, paradoxically results in increased CO and UHC emissions (Lefebvre & Ballal, 2010). This paradox has motivated scientists to search for alternative combustion methodologies and/or control techniques to fulfill the emission standards of CO, UHC, and

---

Received 10 December 2023; revised 31 January 2024; accepted 17 February 2024.  
Available online 20 May 2024

<sup>\*</sup> Corresponding author at: Continuous Combustion Laboratory, Department of Mechanical Power Engineering, Faculty of Engineering – Mataria, Helwan University, Cairo 11718, Egypt.  
E-mail address: [moustafaahmed1411@gmail.com](mailto:moustafaahmed1411@gmail.com) (M.A. GamalEldin).

<https://doi.org/10.62537/2974-444X.1003>

2974-444X/© 2024, Helwan University. This is an open access article under the Creative Commons Attribution-NonCommercial-NoDerivatives licence (CC BY-NC-ND 4.0).

NO<sub>x</sub> for either diffusion or premixed modes of combustion.

Effective mixing within the primary combustion zone is critical for reducing CO emissions. Among the various techniques, jet mixing stands out as highly effective, creating a homogeneous air/fuel mixture through intense vortices, enhancing combustion efficiency and reducing pollutant production. Jets, however, accelerate the action of fresh air and hot gases engaging in the intermediate combustion zone, which rates up soot oxidation and converts any dissociated species into normal species. Furthermore, it entrains more hot combustion gases into fresh reactants, promoting ignition due to mixture preheating but slowing down the reaction rates due to the difficulty of fuel–air meeting (Lefebvre & Ballal, 2010).

In systems termed as ‘colorless distributed combustion,’ flameless oxidation, high-temperature air combustion, and moderate or intense low oxygen dilution (MILD), the fresh fuel and air are mixed and heated by the recirculated exhaust gases before they reach the reaction zone. Accordingly, this creates a uniform and dispersed reaction zone having an almost uniform temperature distribution (with no temperature peaks), leading to low NO<sub>x</sub>, CO, and UHC emissions. These systems also offer fuel flexibility, reduced noise, and require no combustor modification (Arghode & Gupta, 2010, 2013; Khalil & Gupta, 2011a, 2011b, 2013; Lammel et al., 2010; Weber et al., 2004; Wüning & Wüning, 1997).

Ongoing research explores the impact of different geometrical arrangements and air/fuel injection schemes on flow fields and combustor performance to achieve distributed reactions throughout the combustor volume (Khalil et al., 2012, 2013; Khalil & Gupta, 2014a, 2014b).

Air injection can be achieved by different methods, including (i) swirl air injection near fuel injection and (ii) primary, secondary, and dilution air injection downstream. Air injection can enhance the mixing and dilution of the fresh reactants with hot combustion products, which increases the reactant dilution ratio, a key parameter to achieve MILD combustion. Air injection can also increase the turbulence energy of the ambient air and promote air entrainment into the spray flame, which improves combustion performance and efficiency.

A comprehensive investigation into fuel jet trajectory in cross-air flow (Li, Yuan, Varsegov, et al., 2021; Li, Yuan, Yao, et al., 2021; Li et al., 2017) found that elevated turbulent kinetic energy along the trajectory results in rapid fuel mixing, achieving more than 90% local combustion efficiency at the recirculation

#### Nomenclature

MILD	moderate or intense low oxygen dilution
$Q_{in}$	input thermal power, kW
$X_{inj}$	axial location of air injector measured from the stabilizer disk level, cm
$\lambda$	excess air factor

zone boundaries and 99% at its end. Hydrocarbon concentrations peak near the fuel injection port and sharply decrease downstream due to residence time limitations. Minimum CO concentration occurs in the lower velocity zone, allowing complete CO oxidation. The study underscores the intricate interplay of air injection and fuel dynamics in influencing combustion efficiency in MILD combustion.

In addition, Huang et al. (2022) explore the impact of equivalence and staging ratios on a combustion system based on the MILD combustion concept, highlighting the effectiveness of staged combustion in achieving a distributed reaction zone leading to ultra-low NO<sub>x</sub> and CO emissions under lean operating conditions, and the later finding suggested that the NO<sub>x</sub> reduction mechanism is superior to the NO<sub>x</sub> formation mechanism in the MILD combustion zone.

The investigation into the internal entrainment of reactive gases, as conducted by Khalil and Gupta (2016) utilizes experimental studies to simulate recirculated gases by a mixture of N<sub>2</sub> and CO<sub>2</sub> and examines their impact on thermal flow field uniformity and pollutant emissions. Results show an 80% reduction in NO and CO emissions, as well as a reduction in OH chemiluminescence, confirming the establishment of distributed combustion across the combustor. Moreover, Karyeyen and Ilbas (2020) emphasizes that entraining more combustion products into the reaction zone reduces oxygen concentration, slowing the reaction rate and lowering the flame peak temperature. This approach facilitates distributed combustion, leading to low levels of NO<sub>x</sub> emissions and alleviating flame instabilities without requiring additional burner or combustor modifications.

Transverse jets in supersonic crossflow, particularly pulsed jets, are recognized for their efficiency in enhancing the heat release rate of the diffusion flame (Zhao et al., 2021). An experimental and computational study (Sharma et al., 2020) investigated the burning of kerosene fuel in a novel combustor design, employing a staged air concept in the primary, secondary, and dilution flame zones. Co-flowing air in the primary and secondary zones established a distributed combustion zone, leading

to enhanced mixing effectiveness, preheating of reactants, and reduced exhaust emissions ( $\text{NO}_x$ , CO, and CH). Adjusting the injected air's momentum to achieve a global equivalence ratio of between  $\Phi = 0.8$  and  $0.7$  resulted in significant reductions in  $\text{NO}_x$  emissions, with CO emissions maintained at 15–20 ppm.

In another investigation (Tao & Zhou, 2020), the crossflow injection of a  $\text{CO}_2$  and  $\text{O}_2$  mixture through microjet tubes into the root of an ethanol spray was studied for its impact on flame stability, CH, and  $\text{NO}_x$  emissions. Varying axial locations and flow rates of injected jets demonstrated the effectiveness of jets in crossflow injection in augmenting vortex generation, promoting rapid fuel spray vaporization, and reducing combustion instabilities and exhaust emissions. The study recommended early and/or late jet air injection at the flame roots and tail, favoring the reduction of thermal  $\text{NO}_x$  emissions. The preference for jet crossflow injection over streamwise injection was strongly advocated based on experimental observations and analyses.

Uhm and Acharya (2004, 2006) proposed an enhanced strategy for controlling combustion oscillations in a swirl-stabilized spray combustor, incorporating measurements of wall pressure and CH chemiluminescence. This approach utilized a high-momentum air jet to modify the reactant mixing process.

In a separate investigation, Murat Altay et al. (2010) examined the effectiveness of steady air injection near the flame anchoring zone in a backward-facing step combustor to mitigate thermoacoustic instabilities. Two air injection schemes were compared, with cross-stream injection creating a stable flame by generating an intense recirculation zone, and streamwise injection eliminating thermoacoustic instability at an optimum secondary air flow rate.

Deshmukh and Sharma (2017) conducted experiments on a Rijke tube to study thermoacoustic instabilities and their suppression through radial injection of a small fraction of incoming airflow through micro jets. The study recommended radial micro jet injection into the flame for its simplicity and effectiveness in controlling thermoacoustic instability.

This paper presents a novel technique for enhancing the mixing and combustion efficiency of oil diffusion flames by injecting multiple air jets into the core region of the flame. The technique is based on a coaxial disk stabilized burner with multi-annular air injection jets that can vary their axial location and angle. The paper describes the experimental setup and the test cases that vary the axial

location of the air injection jets and the excess air factor at a fixed thermal load of 65 kW. The measurements cover visual flame images, the inflame thermal structure, the heat flux and cumulative heat transfer, and the combustion efficiency and exhaust emissions for each test case. The paper compares the combustion modes of the conventional disk stabilized flame and the air-jet-assisted flame and discusses the transition from diffusion flame to partially premixed flame and MILD combustion.

## 2. Experimental test rig and instrumentation

Fig. 1 illustrates the configuration of the current experimental test facility. This facility consists of a horizontal cylindrical combustor with an inner diameter of 20 cm and a segmented water-cooled jacket comprising 14 segments. To facilitate inflame measurements, the combustor is equipped with 18 measuring taps (6 mm diameter). At the entry of the combustor, a disk-stabilized novel burner, as depicted in Fig. 2, is coaxially mounted. The burner gun, with a diameter of 12 cm, features a central pressure jet atomizer (solid cone: 1.5 gph,  $45^\circ$ ) and is surrounded by a circular stabilizer disk with a diameter of 10 cm, resulting in a blockage ratio of 0.8. This disk is positioned 5 cm from the top end of the burner.

The burner design allows for the inward injection of multiple air jets, with the present work utilizing four such jets. These jets emerge through four stainless steel fine tubes ( $d = 1.5$  mm), which protrude through the stabilizer disk and are evenly spaced at a circumferential circle ( $d = 65$  mm). The axial positioning of these jets, up to 5 cm from the face of the stabilizer disk, is facilitated by a screw-and-nut mechanism that moves the compressed air reservoir carrying the air injection tubes. The top end of each tube is shaped to inject the air at an angle of  $60^\circ$  to the vertical axis. The secondary air stream is sourced from a 5-kW centrifugal blower, and the injected air stream is facilitated by an air-compressed line from the reservoir of a reciprocating compressor.

These design features enable the premixing of the fuel spray, secondary air, and injected air within the recessed volume created between the stabilizer disk and the top end of the burner gun. The degree of premixing and, consequently, the combustion characteristics are influenced by the axial positioning of air injection tubes.

The flow rates of the secondary air and injected air are measured using calibrated orifice plates, with the corresponding differential pressure displayed on a digital manometer. The estimated percentage

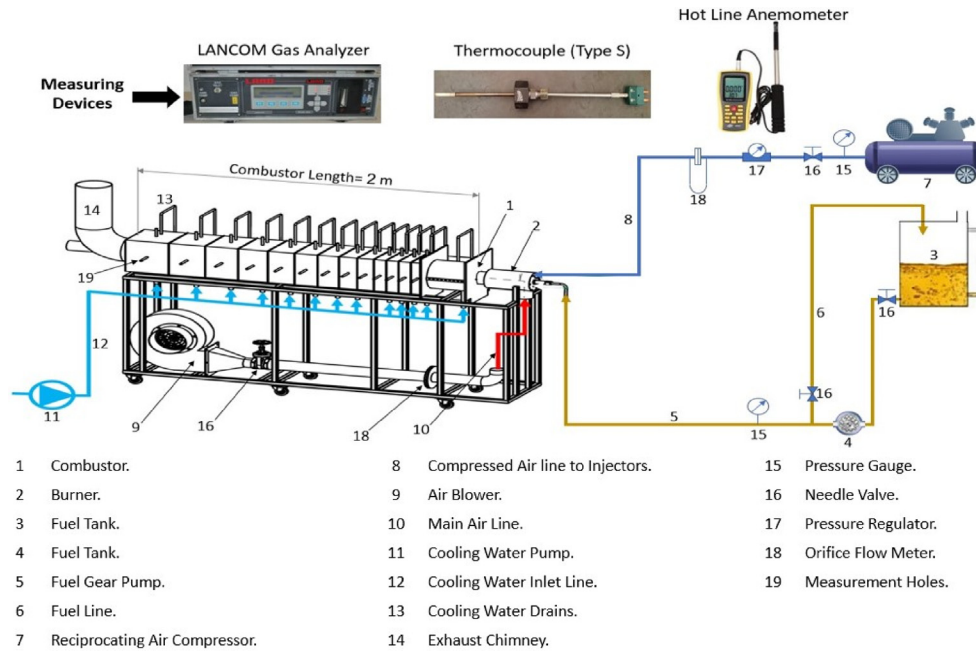


Fig. 1. Experimental test rig.

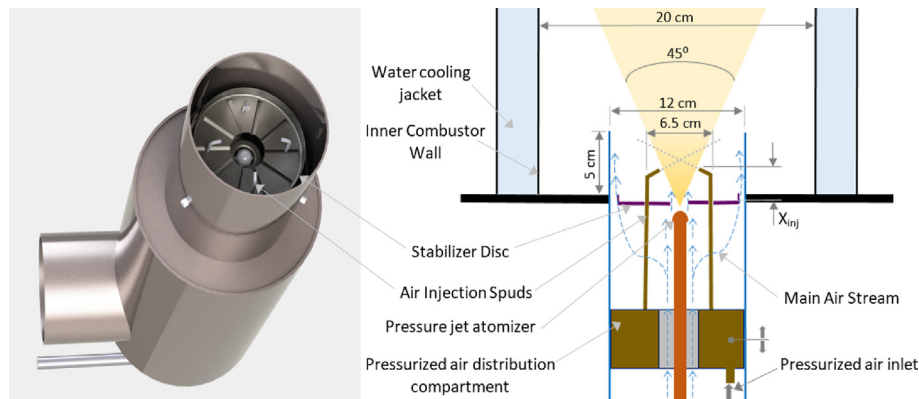


Fig. 2. Schematic sketch of the burner gun as mounted on the water-cooled cylindrical furnace.

error for these measurements is within 3%. The flow rate of the oil through the atomizer is metered using a calibration curve (flow rate vs. pressure), where, at a given pressure, the oil is collected ( $\sim 1$  l) over a specified time.

The employed measuring techniques encompass the following methodologies:

- (1) The determination of the in flame mean gas temperature involves the utilization of a bare fine wire thermocouple (type S,  $150 \mu\text{m}$ ). This approach effectively mitigates the impact of radiation errors, rendering them insignificant and comparable to the repeatability of measurements.
- (2) The assessment of in flame dry volumetric gas analyses for chemical species ( $\text{CO}$ ,  $\text{NO}_x$ , and  $\text{O}_2$ ) is conducted through a stainless-steel water-cooled sampling probe coupled with a LANCOM gas analyzer (AMETEK Land, Dronfield, United Kingdom).
- (3) Measurement of the local mean bulk axial velocity in the air flow field of the cold study segment within the experimental program employs a hot wire anemometer (Benetech GM8903, Benetech, Shenzhen, China).
- (4) For the analysis of vertical free flames and the definition of flame regimes, visual flame images are captured using a digital professional

camera (NIKON Model D5100-16.2-megapixel, Nikon, Tokyo, Japan) at a shutter speed of 0.25 s.

### 2.1. Experimental program

The experimental program was meticulously structured to scrutinize the impact of varying the air injection location on combustion efficiency and exhaust emissions. This scrutiny was accomplished through both visual analysis of flame appearance in free combustion and comprehensive experimental measurements conducted in confined conditions. The focal points of the investigation encompassed the flame's thermal structure and the velocity profiles of the air cold flow.

All experimental analyses transpired under consistent conditions, specifically at an ambient temperature of 27 °C, normal atmospheric pressure of 101 kPa, and a relative humidity of 65%. The prescribed parameters for the study included a constant input thermal power of  $Q_{in} = 65$  kW and a persistent momentum of injected air, featuring a jet velocity of 126 m/s. The volume of injected air, constituting 4% of the theoretically required air for complete combustion, was deducted from the total main combustion air (Table 1).

These conditions were rigorously adhered to, ensuring a standardized and controlled environment for the investigation. The results, thus, offer a nuanced understanding of the interplay between air injection location, combustion efficiency, and exhaust emissions, as evidenced by both visual observations and quantitative measurements in confined settings.

The test cases are implemented across four distinct configurations, as delineated in Table 2. Configuration (R) represents a scenario wherein no air jets emanate from the injectors, resembling the conventional mixing configuration of the stabilizer disk model. The subsequent three configurations, denoted as jet mixing configurations, feature air injection at different locations. Configuration (A) positions the outlet of air injectors 1 cm from the stabilizer disk, configuration (B) places it at 3 cm, and configuration (C) locates it at 5 cm.

Table 1. Physiochemical properties of used fuels.

Parameters	Value
Fuel chemical composition (%wt.)	C: 86.5% H <sub>2</sub> : 13.2% O <sub>2</sub> : 0.2%
Fuel calorific value (mj/kg)	44
Density (kg/m <sup>3</sup> ) at 25 °C	834
Kinematic viscosity (mm <sup>2</sup> /s) at 40 °C	2.6
Stoichiometric air–fuel ratio	14.3

The present study encompasses an examination of 12 cases, systematically varying two parameters, namely  $\lambda$  and the axial location of air jets. These cases and their corresponding configurations are detailed in Table 2.

## 3. Results and discussion

### 3.1. Visual flame structure

Fig. 3 presents photographic images of oil flames under a fixed thermal input of 65 kW, depicting both the reference case (without air injection spuds) and cases with air injection spuds. The experiments were conducted in an open atmosphere, with variations in the axial location of air injection jets (horizontal rows) and different excess factors ( $\lambda = 1.2, 1.4,$  and  $1.6$ ) represented in vertical columns. The bottom row of Fig. 3 illustrates the cold flow field of the mean bulk axial velocity at  $\lambda = 1.6$ . These additional data serve to elucidate the variations in flame regimes for specific test cases (R3, A3, B3, and C3).

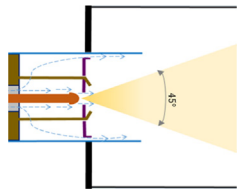
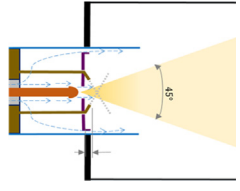
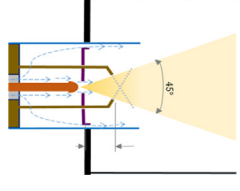
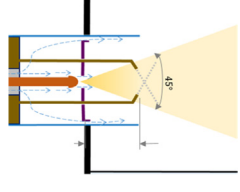
The ensuing observations and elucidations can be gleaned from Fig. 3:

#### 3.1.1. Reference test cases (R1, R2, R3), no air jets (first column)

The evolving flames, progressing from bottom to top, manifested the characteristic sequential stages of soot inception, soot growth, and soot oxidation, regardless of the excess air factor ( $\lambda$ ). Given a constant spray pattern emanating from the fuel nozzle, the incremental augmentation of the surrounding secondary air flow rate (at high  $\lambda$ ) precipitated an accelerated premixing process with the fuel droplets. Consequently:

- (1) The visible flame length was shortened, and the flame width broadened, in accordance with expectations.
- (2) The soot inception zone experienced an acceleration, ultimately terminating within the core of the premix chamber.
- (3) The soot partial oxidation zone demonstrated improvement, evident in the progressive transition from dark brown to a lighter yellowish color.
- (4) The soot oxidation zone's lengthening, broadening, and shift toward the region proximal to the burner exit were observed, marked by a white color within the flame core.
- (5) Pyrolyzed fuel droplets escaping to the outer flame boundaries (light brownish color) underwent slower partial oxidation along these boundaries. The degree of their partial oxidation

Table 2. Test cases at fixed input load of  $Q_{in} = 65 \text{ kW}$ .

Test case	LPG/LDO (%)	Axial location of air injection jets ( $X_{inj}$ )	Excess air factor ( $\lambda$ )	Injected air (kg/h)	Secondary air (kg/h)	Schematic configuration
R1	0	No Air Jet (reference case)	1.2	0.0	97.2	
R2	0		1.4		113.4	
R3	0		1.6		129.6	
A1	0	1 cm	1.2	3.2	94.0	
A2	0		1.4		110.2	
A3	0		1.6		126.4	
B1	0	3 cm	1.2	3.2	94.0	
B2	0		1.4		110.2	
B3	0		1.6		126.4	
C1	0	5 cm	1.2	3.2	94.0	
C2	0		1.4		110.2	
C3	0		1.6		126.4	

seemed to correlate with the excess air factor, aligning with expectations.

### 3.1.2. Variation of axial locations of air injection jets: runs (A1, B1, C1), (A2, B2, C2), and (A3, B3, B4)

The introduction of high-momentum air jets at acute angles ( $60^\circ$ ), directed toward the central region of the flame, results in an approximate 50% reduction in visible flame length when compared with reference cases with no air jets. In addition, the flame's shape, appearance, and regimes undergo substantial changes, contingent upon both the location of the injected air jets and the excess air factor. These alterations arise from the formation of intense vortices through interactions between the high-momentum air jet and the central oil spray within the premix chamber. These vortices manifest in diverse forms, including counter-rotating pairs, shear vortices, wake vortices, and horseshoe vortices.

However, the stabilizer disk at the entry of the premix chamber introduces an additional central

recirculation zone, comprising hot combustion products from downstream. These configurations promote rapid vaporization of the fuel spray and the generation of a premixed mixture of fuel and air within the premix chamber. The extent of premixing, the mixture strength, and its residence time in the premix chamber are substantially influenced by the location of the injected air ( $X_{inj}$ ) and the excess air factor ( $\lambda$ ).

The aforementioned analyses provide the foundational understanding necessary to elucidate changes in flame shape, appearance, and regimes at varying air injection locations and excess air factors (refer to Fig. 3). The observed phenomena are explicated as follows.

The reduction in flame length associated with air injection is attributable to the transition from a diffusion flame (in the absence of air injection) to a lean partially premixed flame (with air-jet injection).

Changes in flame shape, appearance, and regimes are explicable through an examination of the air velocity field exiting the premix chamber, as



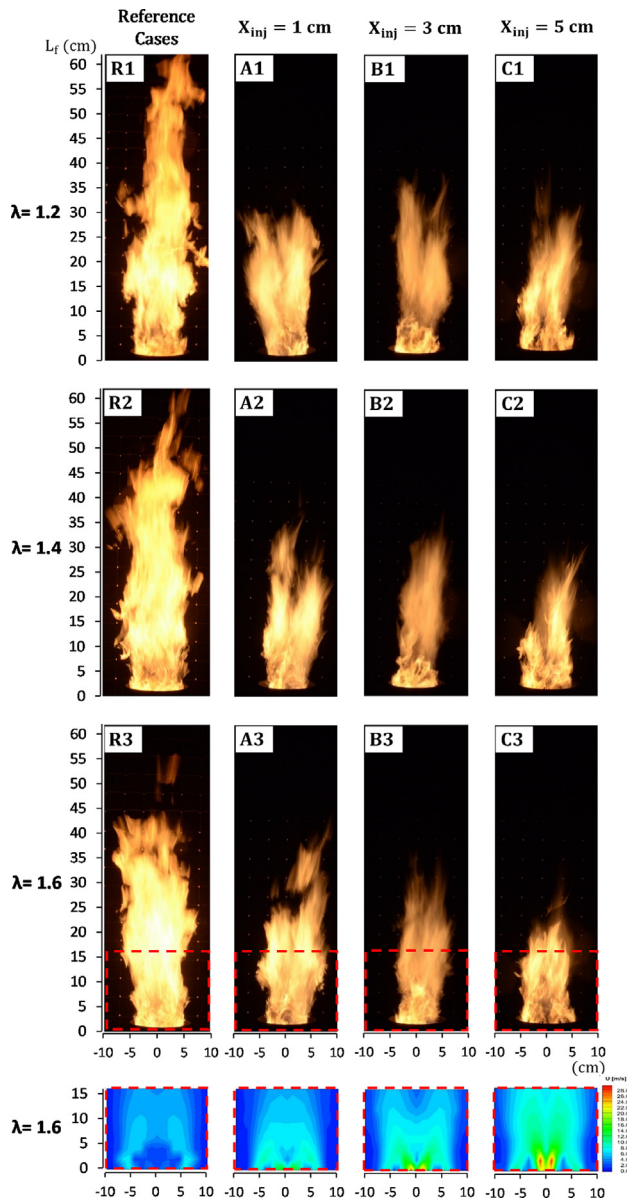


Fig. 3. Flame visual images at fixed thermal input loading (65 kW), varying axial location of the air penetrating jets (horizontal rows), and different excess air factors (vertical columns); row 4 illustrates the mean bulk velocity on a cold air velocity when using the same amount of air as in  $\lambda = 1.6$ .

illustrated in row 4 of Fig. 3, for instance, in the case of  $\lambda = 1.6$ . The following observations can be deduced:

(1) In case of no air injection (first LHS image).

A prominent central recirculation zone dominates the central core region, discernible by its dark blue hue. Surrounding this zone is a concise envelope of high velocity, emanating from the stabilizer disk and converging inwardly toward the flame core.

This configuration facilitates expeditious fuel pyrolysis and its subsequent admixture with air within the core region, thereby fostering accelerated oxidation of soot. The temporal manifestation of the soot oxidation zone (identified by its bright white color) is contingent upon the excess air factor. Notably, in runs R1, R2, and R3, depicted in the first column of Fig. 3, a direct correlation is evident between a higher excess air factor and an earlier onset of the soot oxidation zone.

(2) In case of air injection (second, third, and fourth images from LHS)

(a) At the lowest air injection location ( $X_{inj} = 1$  cm) (depicted in the second column).

The introduced air infiltrates the central recirculation zone within the premix chamber, manifesting as an annular pattern at the immediate exit of the premix chamber, characterized by a higher velocity and a light green coloration. This phenomenon results in the bifurcation of the developed flame into four longitudinal annular quarters. This spatial reconfiguration promotes the rapid transition to soot oxidation, facilitated by the creation of an expanded surface area conducive to the swift oxidation of the partially oxidized fuel/air mixture. Importantly, the extent and location of the soot oxidation zone exhibit sensitivity to the excess air factor ( $\lambda$ ), with a greater excess air factor correlating with a more pronounced shifting and broadening of the soot oxidation zone, closer in proximity to the burner exit.

(b) (At the intermediate air injection location ( $X_{inj} = 3$  cm) (depicted in the third column).

At the intermediate air injection location, denoted as  $X_{inj} = 3$  cm, and corresponding to the images in the third column, the air injection point intersects the central atomized spray at approximately the mid-height of the premix chamber. This spatial arrangement occurs where the fuel droplets have undergone partial vaporization. The consequence of this configuration is twofold: it promotes an early and accelerated premixing between the fuel and air, yet concurrently diminishes the residence time required for achieving the desired mixture strength and homogeneity at the premix chamber exit.

Consequently, the resultant mixture undergoes partial oxidation within the premix chamber, manifested by a discernible yellowish bright core enveloped by a light brownish halo. The remaining

partially combusted mixture experiences a protracted reaction downstream, indicated by a light brownish hue, until reaching visible flame length. This prolonged reaction is attributed to the lower probability of air availability in a dense, partially oxidized species. Altering the excess air factor ( $\lambda$ ) from 1.2 to 1.6 (observed in runs B2 and B3) induces marginal enhancements in mixture reactivity, leading to a reduction in visible flame length and an expansion of flame width, though not to the extent anticipated. This intermediate injection location exhibits unfavorable characteristics, as elucidated in subsequent sections.

(c) At the highest air injection location ( $X_{inj} = 5$  cm) (depicted in the fourth column).

Moving to the highest air injection location,  $X_{inj} = 5$  cm, and corresponding to the images in the fourth column, the injected air is positioned at the premix chamber exit plane. Consequently, the central fuel spray undergoes earlier vaporization and seamlessly integrates inside the premix chamber, with the annular air stream around the stabilizer disk and the hot recirculated gases within the central recirculation zone. This intricate interaction results in the prompt formation of a well-mixed combination of air, vaporized fuel droplets, and hot recirculated combustion products.

This well-mixed amalgamation attains further homogeneity and air availability at the immediate premix chamber exit, leading to rapid reactions following the premixed combustion mode. Consequently, the ensuing flames exhibit significantly reduced lengths with a rapid development of a brighter soot oxidation zone, observed in runs C1, C2, and C3. Elevating the excess air factor ( $\lambda$ ) from 1.2 to 1.6 intensifies the reaction zone, culminating in a shortened visible flame length and a broadened flame width.

It is imperative to note that preheating the airlines emerges as a critical factor, facilitating rapid mixing and precluding the possibility of quenching effects induced by cold air streams.

### 3.2. The inflame thermal structure

#### 3.2.1. Axial variations of the mean gas temperature

Fig. 4 shows on-axis variations of the mean gas temperature for all the test cases given in Table 2. Temperature measurements started at the immediate exit of the premix chamber are extended all through the combustor length. The presented data

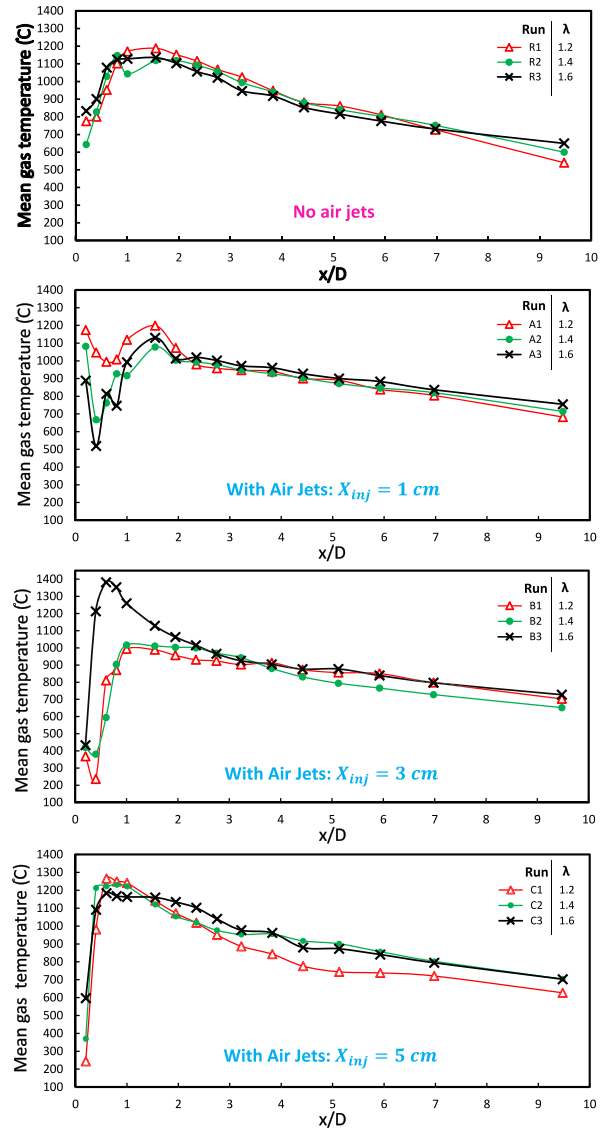


Fig. 4. Axial distributions of the inflame mean gas temperature at different excess air factor.

seem to provide a clear insight into the axial variations of the degree of mixing within the premix chamber and hence the combustion mode within the flame core. This may be illustrated for each test case as follows:

(1) Reference case, nonexistence of injected air (runs: R1, R2, and R3).

The mean gas temperature at the immediate exit of the burner ranges between 600 and 800 °C. This indicates partial premixing between the vaporized fuel droplets, the secondary air issuing from the annulus area surrounding the stabilizer disk and the incoming recirculated hot combustion products

with the central recirculation zone. This is a typical situation of a stabilized diffusion flame (mixing controlled) that leads to partial oxidation of reactants. This is followed by a gradual rise in temperature leading to a maximum temperature plateau of only 1200 °C (within the soot oxidation zone) and followed by a gradual fall (due to heat loss) to reach a level of 700 °C near the combustor exit ( $x/D = 9$ ).

(2) Early injection of air jets ( $X_{inj} = 1$  cm) (runs: A1, A2, and A3).

The mean gas temperature at the immediate exit of the premix chamber exhibits comparatively higher levels of temperature ranging from 1200 °C (at  $\lambda = 1.2$ , run A1) to 900 °C (at  $\lambda = 1.6$ , run A3). This finding suggests the early occurrence of partially premixed combustion (zone 1), within the premix chamber that resulted in the rapid disintegration of the injected oil spray to finer droplets that subsequently undergo rapid premixing with the injected and secondary air streams (within the full length of the premix chamber), leading to rapid premixing and partial oxidation. The exiting mean gas temperature attained at the exit of the premix chamber drops with the air dilution associated with the increase of the excess air factor.

This stage is subsequently followed by three subsequent stages, namely:

(a) Stage (2): rapid drop in mean gas temperature ( $0.1 < x/D < 0.3$ ).

whereby the mean gas temperature reaches a lower level of 500 °C (at  $\lambda = 1.6$ ) due to the flow expansion from the burner exit section to the broader combustor volume, the dilution of the remaining reactants (within the flame core) by the recirculated combustion products within the central recirculation zone and the flame radiant heat loss to the combustor cooling jacket.

(b) Stage (3): diffusion mode of combustion ( $0.3 < x/D < 1.5$ ).

The mean gas temperature rises at a lower gradient to reach another maximum level of the order of ~1100–1200 °C just before the location of the visible flame length, depending on the value of  $\lambda$ . The reason stems from the fact that the earlier partially premixed combustion within the premix chamber (zone 1) consumed a smaller portion of the fuel due to the lower burning velocity associated with lean mixtures. As such the remaining unburned fuel (larger portion) had to get mixed with

the available air to be combusted following the ‘mixing-controlled concept’ of a diffusion mode of combustion.

(c) Stage (4): flame tail to end of combustor ( $1.5 \leq x/D \leq 9.5$ ).

This region exhibits a gradual decline of the mean gas temperature due to the convective heat transfer from the exhaust gases to the combustor cooling jacket.

(3) Intermediate injection of air jets ( $X_{inj} = 3$  cm) (runs B1, B2, and B3).

In this case the four air injection jets penetrate the central oil spray at a further downstream location where the spray pattern exhibited finer droplet distribution. As such, it resulted in rapid droplet vaporization and mixing with air that led to the formation of a premixed mixture at the burner exit featuring very little partial oxidation as indicated by a lower temperature of ~400 °C. This is followed by a rapid rise in temperature following a premixed mode of combustion. The maximum flame temperature reaches a maximum of ~1000 °C (for  $\lambda = 1.2$  and 1.4 at  $x/D \approx 1.0$ ) and 1400 °C (for  $\lambda = 1.6$  at  $x/D \approx 0.6$ ). This latter finding suggests greater availability of air within the flame core at a higher excess air factor leading to a shorter flame (as seen in column 3 of Fig. 3), typical of MILD combustion concept.

(a) Late injection of air jets ( $X_{inj} = 5$  cm) (runs C1, C2, and C3).

In this case, the central spray undergoes slower vaporization and partial premixing with the central air stream within the premix chamber and is subjected to rapid penetration by the injected air jet at the immediate burner exit. This situation leads to greater availability of air within the central recirculation zone that leads to a higher reaction rate (following the premixed mode of combustion). This is evident by the steeper temperature rise in the flame temperature, the much shorter and intense flame core, giving higher radiation rates (as seen in column 4 of Fig. 3).

### 3.3. Radial variations of the mean gas temperature

Fig. 5 shows a sample of the radial variations of the mean gas temperature for the test cases of no air jet injection at varying values of  $\lambda$  and fixed axial location within the flame base ( $x/D = 0.8$ ). It is clear that:

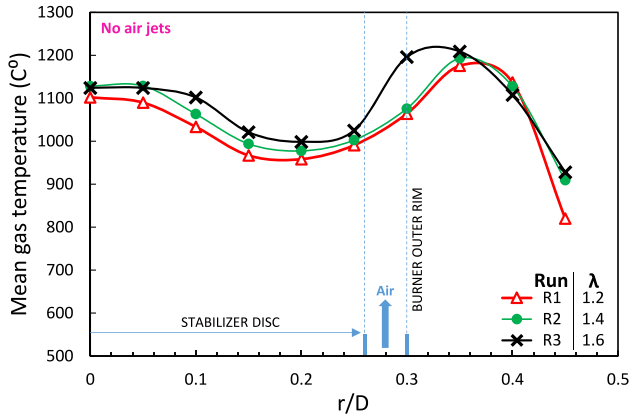


Fig. 5. Radial variations of mean gas temperature, measured at  $x/D = 0.8$ , for reference cases (runs: R1, R2, and R3), no air injection, at varying values of  $\lambda$  and fixed  $Q_{in} = 65$  kW.

- (1) The inner central core region  $0 \leq r/D \leq 0.1$  exhibits a uniform temperature distribution typical of a central recirculation zone. The mean gas temperature is  $1100^\circ\text{C}$ .
- (2) The intermediate region  $0.15 \leq r/D \leq 0.35$  exhibits a diffusion mode of combustion showing a gradual rise of temperature to reach a maximum of  $\sim 1200^\circ\text{C}$  at the flame envelope ( $r/D = 0.33$  at  $\lambda = 1.6$  and  $r/D = 0.35$  at  $\lambda = 1.2$  and  $1.4$ ).
- (3) The outer flame boundaries at  $r/D > 0.33$ – $0.38$  (depending on  $\lambda$ ) is characterized by a gradual decline of mean gas temperature as expected.

Fig. 6 shows a sample of the radial variations of the mean gas temperature for the test cases of air jet injection at varying values of  $X_{inj} = 0, 1, 3,$  and  $5$  cm and a fixed value of  $\lambda = 1.6$  and fixed measuring axial location within the flame base ( $x/D = 0.8$ ). It is clear that:

- (1) Earlier air injection ( $X_{inj} = 1$  cm) resulted in a severe drop of temperature at the flame

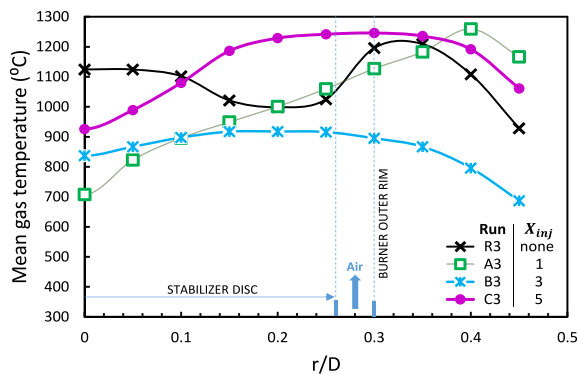


Fig. 6. Radial variations of mean gas temperature, measured at  $x/D = 0.8$ , for reference and air injecting cases at  $\lambda = 1.6$  (runs: R3, A3, B3, and C3) and fixed  $Q_{in} = 65$  kW.

centerline (from  $1120^\circ\text{C}$  in case of no air injection to  $700^\circ\text{C}$ ). This indicates the severe quenching of reaction by the injected air jets and the dilution and/or preheating of air fuel mixture formed by the central recirculation zone due to the stabilizer disk. These lead to the occurrence of limited partial oxidation of the air fuel mixture formed within the premix chamber. The remaining downstream flame regimes exhibited a progressive rise of the flame temperature (following a diffusion mode of combustion) to reach a maximum of  $1250^\circ\text{C}$  at a wider radial location of the flame envelope (giving a comparatively higher level of NOx of  $\sim 40$  ppm, see Fig. 8 below).

- (2) Delayed air injection ( $X_{inj} = 3$  and  $5$  cm) resulted in improving partial oxidation within the flame core region as indicated by the rise of flame temperature (by almost  $120$ – $220^\circ\text{C}$ ) when compared with the above-mentioned case ( $X_{inj} = 1$  cm). This is however much below the case of no air injection (by about  $300$ – $200^\circ\text{C}$ ). This finding gives further indication of the progressive diminishing role of the central recirculation zone within the premix chamber with the progressive increase of axial location of air injection jets.
- (3) The temperature profiles for the cases of delayed air injection location ( $X_{inj} = 3$  and  $5$  cm) showed greater uniformity (i.e. eliminating hot spots) across the developed flames at a temperature level well below the threshold ( $1700$  K) of thermal NOx formation by Zeldovich mechanism.

### 3.4. Heat flux and cumulative heat transfer to the water-cooling jacket

Fig. 7 shows the cumulative heat transfer and the corresponding heat flux variations to the combustor cooling jacket along the combustor for the reference case (runs R1, R2, R3 without air injection jets) and with air injection at different axial locations (runs A1–A3, B1–B3, and C1–C3).

- (1) In the test cases shown in Fig. 7, and irrespective of the variations of  $\lambda$  and/or the injection location of the air jets the following findings may be withdrawn:

- (a) Axial variations of the heat flux exhibit a rapid rise from about  $50$  kW at the immediate exit of the burner to a maximum of  $90 \leq \text{HF} \leq 110$  kW/m<sup>2</sup> at  $x/D \sim 1.75$  for the test case at  $\lambda = 1.2$ . This axial location coincides with the location of the soot

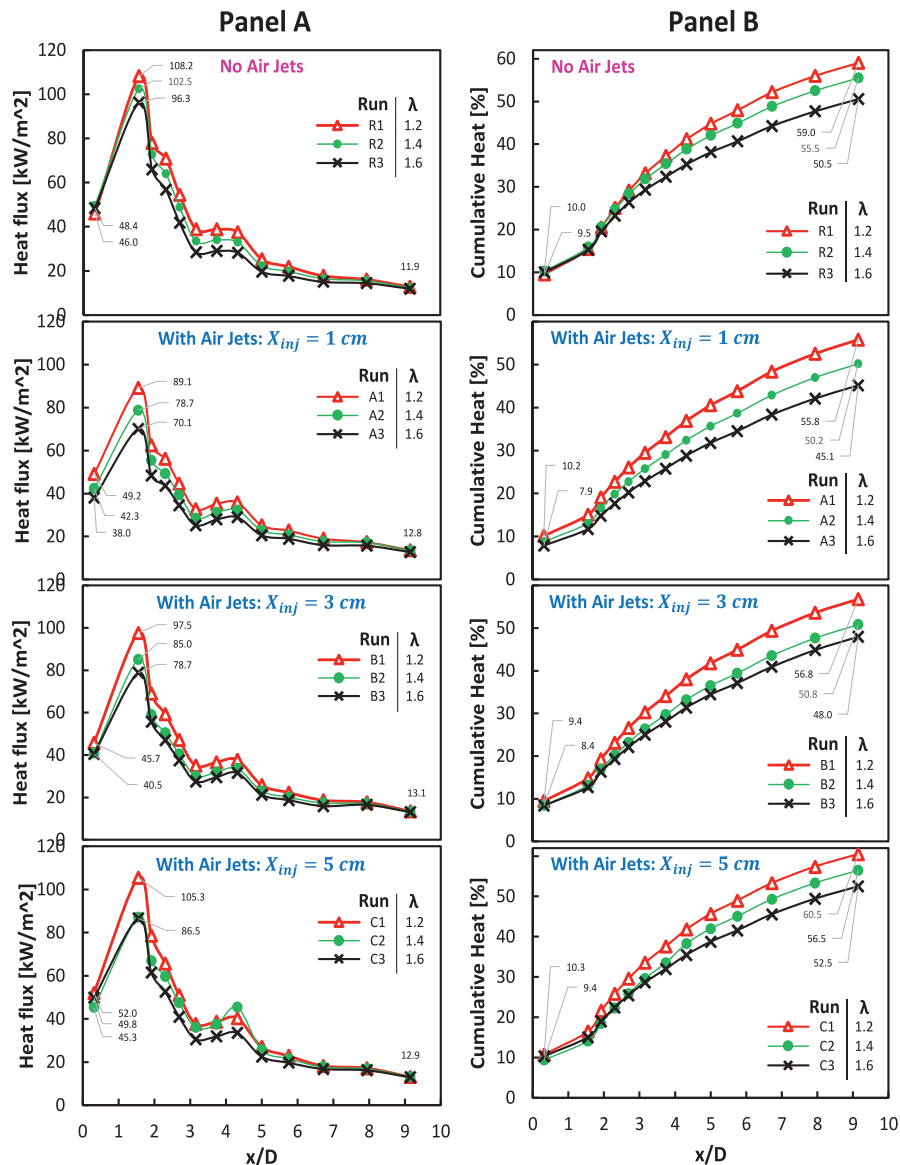


Fig. 7. Logitudinal variations of the combustor wall heat flux (Panel, A) and the cumulative heat transfer to the water-cooling jacket (Panel, B) at different excess air factor ( $\lambda$ ) for varying axial location of the air injection jets ( $X_{inj}$ ) (fixed input power = 65 kW).

oxidation zone (shown in bright white color in Fig. 3). This is followed by a gradual decline to reach a level of  $\sim 40$  kW/m<sup>2</sup> at  $x/D \sim 3$ , where it exhibits a short plateau followed by a slower progressive decline within the exhaust gas regime to a level of 12 kW/m<sup>2</sup> at  $x/D = 9$ .

- (b) The same trend of the heat flux distributions is observed in the test cases having higher values of the excess factor ( $\lambda$ ) but at lower values [runs (R2 and R3) at  $\lambda = 1.4$  and 1.6]. This may suggest the selection of  $\lambda = 1.2$  in view of obtaining higher levels of heat flux, but this selection would be at the

sacrifice of higher levels of CO exhaust emissions and loss of the combustion efficiency as shown in Table 3. Thus, it logically appears that the value  $\lambda = 1.6$  becomes the optimum selection when taking into consideration its provision of the highest combustion efficiency and the much lower CO and NO<sub>x</sub> emissions.

- (2) The percentage variations in the rise of the cumulative heat transfer to the combustor cooling jacket (for all test cases) are shown in panel B of Fig. 7.

(a) Across all test cases, increasing the excess air factor reduces the quantity of heat

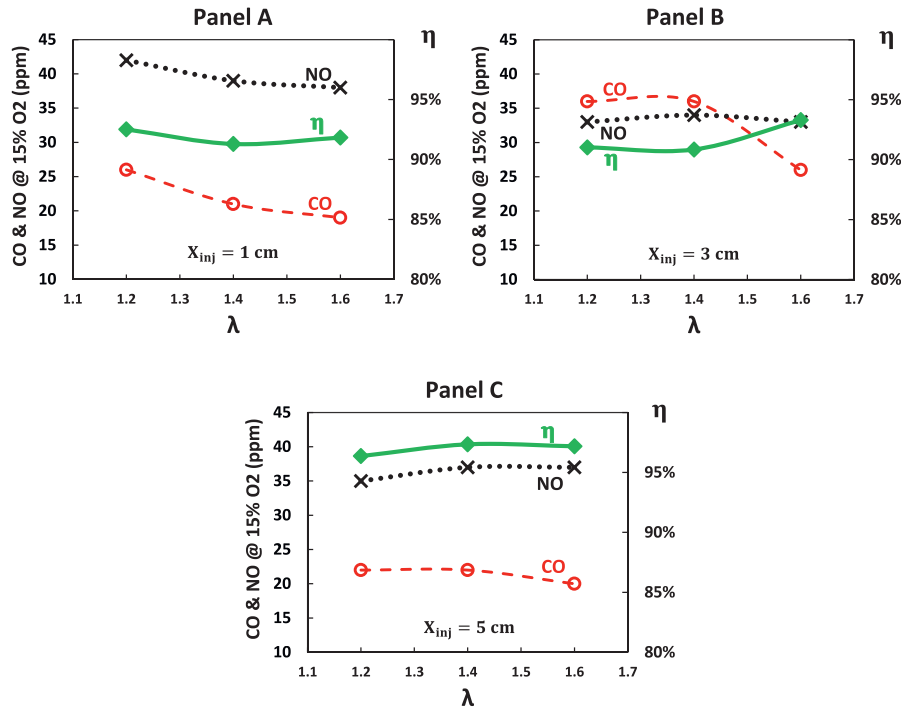


Fig. 8. Variations of the normalized dry volumetric analyses of exhaust emissions of CO and NO<sub>x</sub> together with the combustor efficiency at different values of excess air factor ( $\lambda$ ) and axial location ( $X_{inj}$ ) of air injection jets.

Table 3. Combustion efficiency and exhaust emissions for disk-stabilized configuration without air injection at 65 kW thermal load.

Excess air factor ( $\lambda$ )	1.2	1.4	1.6
CO @ 15% O <sub>2</sub> (ppm)	1015	568	437
NO <sub>x</sub> @ 15% O <sub>2</sub> (ppm)	20	23	26
Combustion efficiency (%)	90	92	95

transferred to the cooling jacket water along the combustor. Although augmenting the volume of air within the combustor enhances heat transfer by convection, the residence time between the combustion products and the combustor wall diminishes due to the small diameter ratio of 1.6 between the combustor and burner rim diameter. This makes the heat transfer to the combustor wall more sensitive to variations in wall tangential velocities, hence affecting the residence time of combustion products. This is clearly reflected in the elevated exhaust gas temperatures in the chimney.

- (b) The heat transfer to the cooling jacket water decreases when the air jets are injected closer to the stabilizer disk at  $X_{inj} < 5$  cm, compared with the reference test cases (runs R1, R2, and R3). However, this trend

changes when the injection position reaches 5 cm, which gives the highest heat transfer percentage for all test cases at  $\lambda = 1.2$ .

### 3.5. Combustion efficiency and exhaust emissions

#### 3.5.1. Cases without air injection jets

Table 3 Variations of the normalized exhaust emissions of CO and NO<sub>x</sub> and the combustion efficiency and at a fixed input thermal load and different excess air factor ( $\lambda$ ) for the reference case (without air jet injection). It is clearly seen that the progressive rise in  $\lambda$  from 1.2 to 1.6 leads to an improvement in fuel/air mixing as indicated by the progressive rise of combustion efficiency (~3%), drop in CO (~43%) and rise in NO<sub>x</sub> (~30%).

#### 3.6. Test cases with air injection jets

On the contrary, the admission of the air injection jets, Fig. 8, causes a dramatic reduction of the CO exhaust emissions (down to ~20 ppm), which is also coupled with an improvement of the combustion efficiency and a rise in NO<sub>x</sub> exhaust emissions. The latter is however seen to be within an acceptable

limit (~30–40 ppm). The results in Fig. 8 clearly indicated that:

- (1) The combustion efficiency ( $\eta$ ) and exhaust emissions of CO and NO<sub>x</sub> at any level of  $\lambda$  are affected by the axial location of the air injection jets ( $X_{inj}$ ).
- (2) The levels of NO and CO emissions decreases with increasing the excess air factor ( $\lambda$ ) at the early air injection ( $X_{inj} = 1$  cm), due to increasing the availability of air which enhances the oxidation rate on one hand and on the other hand dilute the whole flame temperature.
- (3) At the intermediate injection location ( $X_{inj} = 3$  cm), the CO emissions sharply decreases and combustion efficiency notably increases with increasing the excess air factor from  $\lambda = 1.4$ – $1.6$ , which reflects the improvement in the oxidation rate as mentioned in Section 3.1.
- (4) The best axial location of the air injection jets is located at the immediate exit of the burner premix chamber ( $X_{inj} = 5$  cm, panel c in Fig. 8) as it resulted in a comparatively higher combustion efficiency ( $\eta = 97\%$ ), lowest CO emissions ~20 ppm, and a permissible level of NO<sub>x</sub> of ~35 ppm.

#### 4. Conclusions

This paper introduces a novel technique to improve the mixing and combustion efficiency of oil diffusion flames by injecting multiple air jets into the flame core region. The technique uses a coaxial disk stabilized burner with multiannular air injection jets that have adjustable axial positions. The paper describes the experimental setup and the test cases that vary the axial positions of air injection jets and the excess air factor at a constant thermal load of 65 kW. The paper presents the visual flame images, the in-flame thermal structure, the heat flux and cumulative heat transfer, and the combustion efficiency and exhaust emissions for each test case. The paper compares the combustion modes of the conventional disk-stabilized flame and the air-jet-assisted flame and discusses the transition from diffusion flame to partially premixed flame and MILD combustion. The paper reports the following main findings and implications:

- (1) Early air injection jets can:
  - (a) Shorten the visible flame length by nearly 50% and alter the diffusion combustion mode to either an MILD or lean partially premixed combustion.

- (b) Enhance the fuel droplet vaporization and increase fuel/air residence time, and hence the degree of premixing and the soot oxidation are improved.

- (2) The late air injection location at 5 cm from the stabilizer makes the flame characteristics not sensitive to the variation in the excess air factor.
- (3) The optimum location of air injection jets is at the exit plane of the premix chamber (5 cm from the stabilizer disc), which leads to the highest combustion efficiency, the lowest CO emissions, and a permissible level of NO<sub>x</sub> emissions.

The proposed technique can be applied to gas turbine combustion to achieve clean and efficient energy conversion. It can also be applied to other oil diffusion flames with similar burner designs and operating conditions, but further studies are required to optimize the parameters of air injection jets and to examine the effects of different fuels and thermal inputs. Moreover, numerical simulations and modeling are essential to validate and supplement the experimental results and provide more insights into the underlying physics and chemistry of air-jet-assisted combustion.

#### Conflicts of interest

There are no conflicts of interest.

#### References

- Alan, P., Loeb, E., & Nasralla, M. M. (2001). *Review and assessment of air quality standards in Egypt*. Egyptian Environment Policy Program, Program support unit, USAID Contract no. PCE-I-00-96-00002-00 (Task order no. 832).
- Arghode, V. K., & Gupta, A. K. (2010). Effect of flow field for colorless distributed combustion (CDC) for gas turbine combustion. *Applied Energy*, *87*, 1631–1640.
- Arghode, V. K., & Gupta, A. K. (2013). Role of thermal intensity on operational characteristics of ultra-low emission colorless distributed combustion. *Applied Energy*, *111*, 930–956.
- Dareck, M., Edelstenn, C., & Ender, T. (2011). Flightpath 2050 Europe's vision for aviation. *Report of the High Level Group on Aviation Research*, *28*, 14–16.
- Deshmukh, N. N., & Sharma, S. D. (2017). Suppression of thermoacoustic instability using air injection in horizontal Rijke tube. *Journal of the Energy Institute*, *90*, 485–495.
- Huang, M., Li, R., Xu, J., Cheng, S., Deng, H., Rong, Z., et al. (2022). Effect of equivalence ratio and staging ratio on the methane MILD combustion in dual-stage combustor. *Fuel*, *307*, 121903.
- Karyeyen, S., & Ilbas, M. (2020). Application of distributed combustion technique to hydrogen-rich coal gases: A numerical investigation. *International Journal of Hydrogen Energy*, *45*, 3641–3650.
- Khalil, A. E. E., Arghode, V. K., & Gupta, A. K. (2013). Novel mixing for ultra-high thermal intensity distributed combustion. *Applied Energy*, *105*, 327–334.
- Khalil, A. E. E., & Gupta, A. K. (2011a). Distributed swirl combustion for gas turbine application. *Applied Energy*, *88*, 4898–4907.

- Khalil, A. E. E., & Gupta, A. K. (2011b). Swirling distributed combustion for clean energy conversion in gas turbine applications. *Applied Energy*, *88*, 3685–3693.
- Khalil, A. E. E., & Gupta, A. K. (2013). Fuel flexible distributed combustion for efficient and clean gas turbine engines. *Applied Energy*, *109*, 267–274.
- Khalil, A. E. E., & Gupta, A. K. (2014a). Dual injection distributed combustion for gas turbine application. *Journal of Energy Resources Technology*, *136*, 1.
- Khalil, A. E. E., & Gupta, A. K. (2014b). Velocity and turbulence effects on high intensity distributed combustion. *Applied Energy*, *125*, 1–9.
- Khalil, A. E. E., & Gupta, A. K. (2016). Thermal field investigation under distributed combustion condition. In *54th AIAA aerospace sciences meeting*, p. 0496. <https://doi.org/10.2514/6.2016-0496>
- Khalil, A. E. E., Gupta, A. K., Bryden, K. M., & Lee, S. C. (2012). Mixture preparation effects on distributed combustion for gas turbine applications. *Journal of Energy Resources Technology*, *134*, 3.
- Lammel, O., Schütz, H., Schmitz, G., Lückerrath, R., Stöhr, M., Noll, B., et al. (2010). FLOX® combustion at high power density and high flame temperatures. *Proceedings of the ASME Turbo Expo, 2(PARTS A AND B)*, *132*, 1069–1081.
- Lefebvre, A. H., & Ballal, D. R. (2010). Gas turbine combustion: Alternative fuels and emissions. In *Statewide agricultural land use baseline 2015* (Vol. 1). pp. 129–133.
- Li, S., Chen, Z., He, E., Jiang, B., Li, Z., & Wang, Q. (2017). Combustion characteristics and NO<sub>x</sub> formation of a retrofitted low-volatile coal-fired 330 MW utility boiler under various loads with deep-air-staging. *Applied Thermal Engineering*, *110*, 223–233.
- Li, Z., Yuan, Y., Varsegov, V. L., Guo, B., Xiao, B., & Duan, P. H. (2021). Study on the mixing characteristics of circular transverse jet in crossflow. *Aerospace Science and Technology*, *112*, 106599.
- Li, Z., Yuan, Y., Yao, J., Varsegov, V. L., Duan, P. H., & Zhao, L. (2021). Study of circular transverse jet - a new method for high-efficiency mixing and combustion in crossflow. *International Communications in Heat and Mass Transfer*, *123*, 105207.
- Murat Altay, H., Hudgins, D. E., Speth, R. L., Annaswamy, A. M., & Ghoniem, A. F. (2010). Mitigation of thermoacoustic instability utilizing steady air injection near the flame anchoring zone. *Combustion and Flame*, *157*, 686–700.
- Sharma, S., Chowdhury, A., & Kumar, S. (2020). A novel air injection scheme to achieve MILD combustion in a can-type gas turbine combustor. *Energy*, *194*, 116819.
- Tao, C., & Zhou, H. (2020). Effects of different preheated CO<sub>2</sub>/O<sub>2</sub> jet in cross-flow on combustion instability and emissions in a lean-premixed combustor. *Journal of the Energy Institute*, *93*, 2334–2343.
- Uhm, J. H., & Acharya, S. (2004). Control of combustion instability with a high-momentum air-jet. *Combustion and Flame*, *139*, 106–125.
- Uhm, J. H., & Acharya, S. (2006). Role of low-bandwidth open-loop control of combustion instability using a high-momentum air jet-mechanistic details. *Combustion and Flame*, *147*, 22–31.
- Weber, R., Smart, J. P., & Vd Kamp, W. (2004). On the (mild) combustion of gaseous; Liquid and solid fuels in high temperature preheated air. In *International symposium on combustion, abstracts of accepted papers* (Vol. 96). pp. 2623–2629.
- Wüning, J. A., & Wüning, J. G. (1997). Flameless oxidation to reduce thermal NO<sub>x</sub>-formation. *Progress in Energy and Combustion Science*, *23*, 81–94.
- Zhao, M., Li, Q., & Ye, T. (2021). Investigation of an optimal pulsed jet mixing and combustion in supersonic crossflow. *Combustion and Flame*, *227*, 186–201.